Research Paper

The fractal micro mechanics of normal compression

CrossMark

John P. de Bono *, Glenn R. McDowell

University of Nottingham, UK

ABSTRACT

The fundamental fractal micro mechanics of normal compression of granular materials is studied using DEM. This paper examines the emergence of a finite fractal bounded by two particle sizes as stress increases, and the evolution of various definitions of the 'smallest particles'. It is revealed that if particles are categorised according to their coordination number, then the volume of all particles with 4 contacts or fewer is directly proportional to the void space. These particles are called 'critical particles' and are shown, for the first time, to explain quantitatively the voids reduction with increasing vertical stress.
© 2016 The Authors. Published by Elsevier Ltd. This is an open access article under the CC BY license (http://creativecommons.org/licenses/by/4.0/).

1. Introduction

The authors have recently published much work accurately modelling the one-dimensional and isotropic normal compression of sand using the discrete element method [1–3]. The most notable outcome of this work was the development of a new compression law, in which the slope of the normal compression line (NCL) is solely a function of the size-hardening effect of the individual particles. The NCL is linear when plotted on two logarithmic axes, and the compression law is given by:

$$\log e = \log e_y - \frac{1}{2b} \log \frac{\sigma}{\sigma_y} \tag{1}$$

where e is the current voids ratio, e_y is the voids ratio at yield, σ is the current stress, σ_y the stress at yield, and $1/2b$ describes the slope of the compression line, where b represents the size effect on particle strength σ_{av}:

$$\sigma_{av} \propto d^{-b} \tag{2}$$

where d is particle size (diameter). The basis of the above compression law is that a fractal particle size distribution (PSD) emerges as a result of particle crushing during normal compression. It was shown in the authors' previous work, by analysing the distribution of particles and contacts that fractal PSDs do indeed emerge during compression [1]. The first aim of this paper is to provide an in-depth analysis of the development of a fractal particle size distribution produced by particle crushing, and in particular what occurs at the fine end of such a distribution as new particle sizes emerge.

The second is to examine some of the assumptions in and validate the compression law given in Eq. (1), and to quantitatively ascertain which particles determine the current voids ratio.

2. Background to model

The work presented here uses a cylindrical sample, initially 20 mm × 20 mm in size, subjected to one-dimensional normal compression to a stress of 45 MPa. The initial sample consists of 857 spheres, 2 mm in diameter, enclosed within rigid walls. The particles are attributed strengths in terms of octahedral shear stress, q:

$$q = \frac{1}{3}[(\sigma_1 - \sigma_2)^2 + (\sigma_2 - \sigma_3)^2 + (\sigma_1 - \sigma_3)^2]^{1/2} \tag{3}$$

where σ_{1-3} are the average principal stresses within the particle, which are returned by the discrete element software, PFC3D 5 [4]. This breakage criterion was chosen as it provides a convenient measure of particle stress, that can be applied to the case of diametral compression (for which the available particle strength data relates to), while also being able to take into account more complex loading geometries, with multiple contacts. The use of Eq. (2) means that a particle loaded with few contacts will, in general, have a larger stress than one loaded more uniformly with many contacts, and therefore would be more likely to break, which seemed physically reasonable. Fundamentally, this criterion satisfies the requirements of taking into account multiple contacts and leads to the correct normal compression behaviour (i.e. the correct slope of the NCL and fractal particle size distributions [1]).

* Corresponding author.

The strengths are attributed to the particles according to a Weibull distribution, where the modulus, m, is 3.3 and the characteristic strength, q_0 is a function of particle size according to:

$$q_0 \propto d^{-3/m} \tag{4}$$

The characteristic strength, q_0, is a value of strength such that 37% of particles are stronger, and is used as a gauge of the average strength for a particular particle size (it is similar in magnitude and proportional to the mean value of the distribution). Weibull statistics are commonly applied to soil particle fracture [e.g. 5,6], a justification of which can be found in McDowell and Amon [7]. The modelling procedure and breakage mechanism is identical to that used in all of the previous works by the authors' [e.g. 1]. The modulus of 3.3 is obtained from experimental particle crushing tests [8], as are the strengths.

When a particle breaks, it is replaced by two smaller sphere fragments, equal in size to one another, and which together have the same volume as the original sphere, ensuring conservation of mass. Particles always split into 2 fragments, and the size ratio of any new fragment and its 'parent' sphere is constant, regardless of scale. The new fragments overlap to an extent that they are located within the boundary of the original sphere (shown schematically in [1,2,9]). The two new fragments are aligned in the direction of the minor principal stress axis of the breaking 'parent' particle. Although this overlap causes an increase in local pressure, the two fragments move apart in the direction of the minor principal stress, just as would occur for a single particle crushed between flat platens. Particle breakage is implemented by checking all particles at once, and all particles in which the stress is greater than the strength are replaced by fragments. The overlap between new fragments is released immediately upon breakage by completing a number of computational timesteps, during which time the particles are allowed to move apart until the system is stable and has reached equilibrium. In previous work [1], the use of 3 and 4 fragments in a symmetric splitting mechanism was also investigated, and it was found that there were no differences in either the normal compression lines or the ultimate particle size distributions. In additionally, using random, non-symmetrical fragmentation mechanisms (following experimental observations) also results in no differences to the resulting NCL or PSDs.

The sequential modelling procedure begins by applying a macroscopic stress increment to the sample. Particles are then checked and allowed to break if necessary. If any particles break, they are replaced by fragments, which are then allowed to move apart, releasing the energy induced by the artificial overlap. This continues until no further breakages occur, after which the macroscopic stress is *re*-applied. Once a macroscopic stress is achieved

with no subsequent breakage, the simulation continues and the next stress increment is applied. This continues until the simulation reaches a point where the size of the smallest particle renders the timestep too small to be computationally economical, which is at 45 MPa in the simulation presented here.

The macroscopic stress increment used is 125 kPa, and maximum velocity of the upper boundary is limited at 0.1 m/s. Gravity is not applied in these simulations. The voids ratio is calculated using the volume of particles and the volume of the container, and is calculated after the overlap and artificial energy has been dissipated following breakages. Relevant model specifics are given in Table 1, however, for full details on the modelling procedure, including discussion of its limitations, the use of the octahedral shear stress as a criterion, the breakage mechanism, and how the principal stresses are calculated, readers are directed to prior publications [1,2,10].

3. Normal compression results

The DEM normal compression results are given in Fig. 1, along with experimental results for the sand that the strength data is obtained from. The slope of the compression line according to Eqs. (1) and (3) should be approximately 0.5, this ideal slope is shown in the figure by the dashed line. As can be seen, the simulation, as well as the experimental results demonstrates agreement with the slope predicted from the size-hardening law for the particles. The simulation is also consistent with the authors' previous results using the same particle properties (although the current work uses a statistically different sample, of a different shape). The yield stress σ_y is approximately 10 MPa.

Progressive particle size distributions from the simulation are shown in Fig. 2(a), at 5 MPa intervals. The PSDs are shown in the conventional manner: the percentage by mass finer plotted against particle size, on semi-logarithmic axes. To avoid clutter, only the extreme PSDs are labelled in the figure, i.e. at 5 MPa and 45 MPa, the intermediate curves are in consecutive order. Experimental PSDs for the corresponding silica sand are given in Fig. 2(b). The use of a monodisperse initial sample in the simulation allows the

Table 1
Summary of DEM properties for the simulation.

| *General simulation properties*	
Oedometer size: height × diameter (mm)	20 × 20
Contact model	Hertz–Mindlin
Wall friction coefficient	0
Wall shear modulus, G (GPa)	75
Wall Poisson's ratio, v	0.30
Particle friction coefficient	0.5
Particle shear modulus, G (GPa)	28
Particle Poisson's ratio, v	0.25
Particle density (kg/m³)	2650
Initial (largest) particle size, d_1 (mm)	2
Initial no. of particles	857
Initial voids ratio	0.75
Initial particles (d_1) 37% strength (MPa)	37.5
Weibull modulus, m	3.3
Final no. of particles	25,527
Final voids ratio	0.43
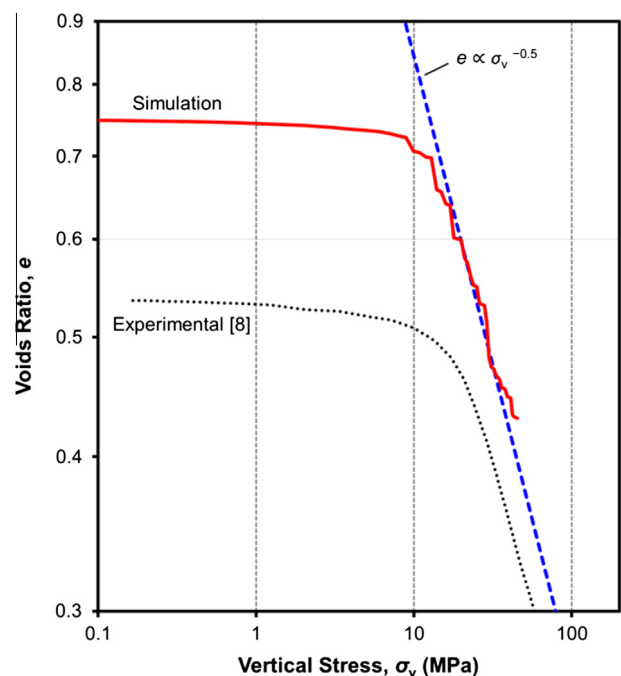
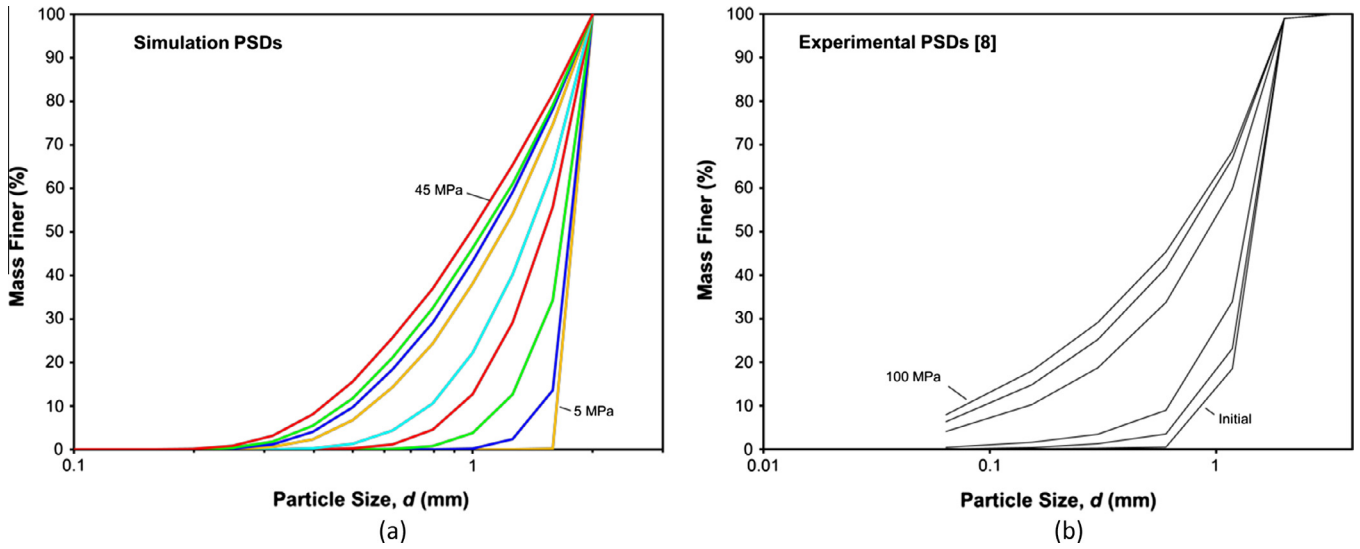**Fig. 1.** Normal compression behaviour for simulation of crushable sand.

Fig. 2. Particle size distributions from the simulation at 5 MPa intervals (a) and from experiments on the corresponding silica sand (b), from McDowell [8].

effects of breakage to be easily observed, however it is worth noting that in previous work [1], the authors investigated using an initially graded sample and results were consistent with experimental observations (the well-graded sample had a different initial voids ratio and yield stress, but both materials had the same normal compression line and ultimate PSDs, which converged at high stresses). It is clear in Fig. 2(a) that substantial crushing takes place, the result being at 45 MPa a smooth grading curve, with an appearance typical of experimental results [e.g. 11–13], and the overall trend is the same as that displayed in Fig. 2(b). As stress increases, the grading curve expands to cover an increasing range of particle sizes, which is effected by a continuously decreasing *smallest* particle size (particles of the largest size remain throughout). The plotted values correspond to the actual particle sizes, i.e. the x-coordinates of the data are 2.0, 1.59, 1.25, ..., 0.079 mm.

To visualise the crushing that has taken place, comparative images of the numerical samples are given in Fig. 3, which show the granular sample before compression (a), and at the terminal stress of 45 MPa (b). The difference is clear, with a vastly greater number of particles and a smaller sample volume in (b). Also shown in (c) is a cross-section of the crushed sample, which gives

a view of the distribution of various particle sizes inside the sample.

4. Fractal distribution

As mentioned in the introduction, the foundation of the compression law in Eq. (1) is that a fractal PSD emerges during compression, with a fractal dimension (D) of 2.5. A fractal particle size distribution is one in which the number of particles, N, of size L, that are greater than a size d, can be expressed as:

$$N(L \geqslant d) \propto d^{-D} \qquad (5)$$

If this relation is plotted on logarithmic axes, then the fractal dimension D is revealed as the slope of the grading curve. It is well documented that compression of granular materials results in fractal particle size distributions, exhibiting fractal dimensions in the region of 2.0–3.0, remarkably usually 2.5 [11,14–16]. Progressive results are shown using logarithmic axes in Fig. 4, again at 5 MPa intervals.

The first thing to note in Fig. 4 is that as the macroscopic stress increases, the y-intercept of the PSD moves upwards, due to an
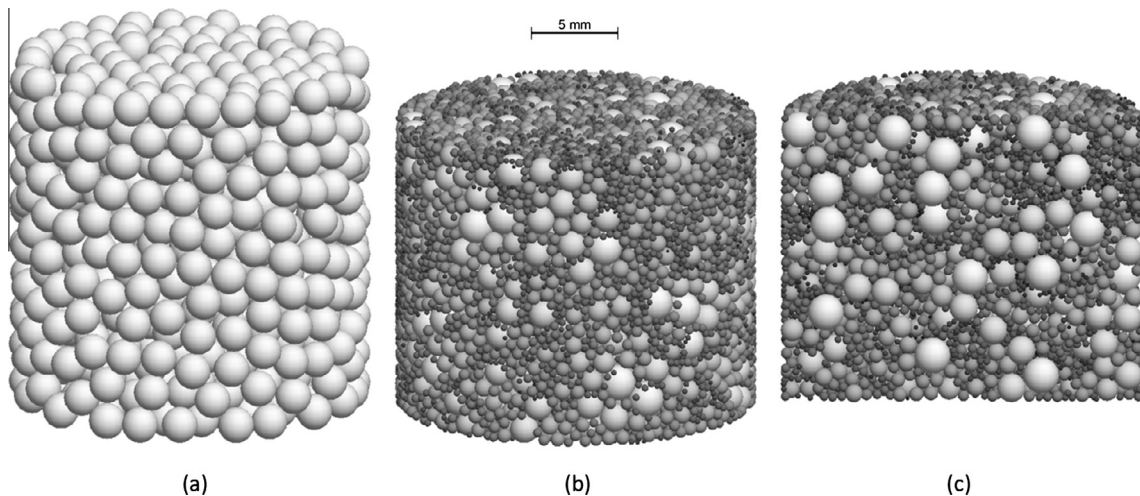

Fig. 3. Images of the sample before compression (a), after compression to 45 MPa (b), and corresponding cross-section of the crushed sample (c), the shades indicate the size/generation of particle, white representing the largest, black the smallest.
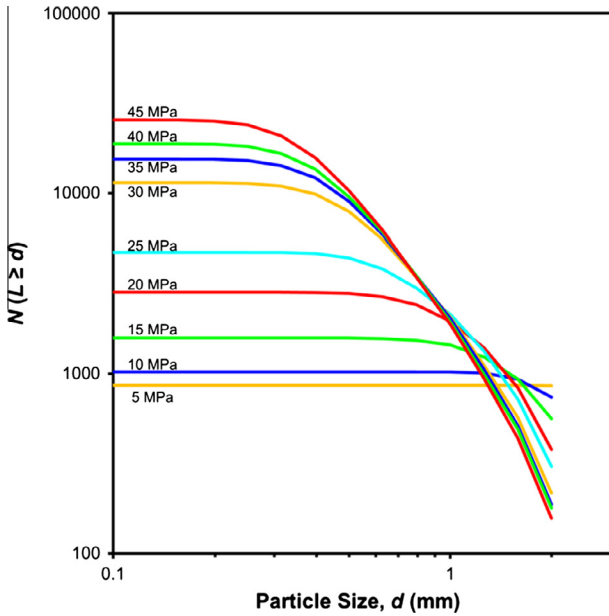
Fig. 4. Evolution of fractal particle size distribution.

increasing total number of particles in existence. Also, the inclined section of the PSD becomes steeper, and covers an expanding range of sizes. This behaviour is the same as that shown previously by the authors as well as others modelling particle breakage using DEM [1,5,17]. The horizontal, left-hand section of each data curves represents sizes *smaller* than the range of particle sizes in existence. The right-hand, inclined section represents the fractal distribution of particle sizes, and this section of the PSD becomes approximately linear after 30 MPa, thereafter appearing to exhibit a constant slope, implying fractal particle geometry. This slope is approximately 2.7 for the data at 45 MPa, slightly larger than the expected value of 2.5, although still in an acceptable range, given that this may be attributed to the finite nature of the discrete distribution, in particular the slightly increased gradient across the largest particle sizes, and this will be addressed shortly. Also note that after the vertical stress of 30 MPa, there are virtually no significant changes to the quantities of particles that lie on the linear, fractal part of the PSD.

According to the definition, a strict fractal distribution would be infinite (i.e. span all particle sizes), but in reality a fractal PSD for a soil must be limited [18], and is bounded by a largest and smallest particle size. Naturally, the largest particle size in this simulation is 2 mm (the size of the original, unbroken particles). If the size of these largest particles is d_1, then the fragments produced directly by any of these particles breaking will have a diameter d_2 (= $d_1 \times 0.5^{(1/3)}$)—where d_2 is the next-smallest size after d_1. The continuing breakage of fragments produces a discrete distribution with particle sizes $d_1, d_2, d_3, \ldots, d_s$, the latter being the smallest particle size in the sample. The subscript denotes what can be termed as the 'Rank' of the particle, i.e. the original (and largest) particles are the 1st rank, their direct fragments comprise the 2nd rank, and so on, up until the smallest rank of particles, which consists of the particles that are of the smallest size d_s.

For such a discrete distribution, for any given rank (size) of particle, the number of particles larger can be expressed as:

$$N(L \geqslant d_i) \propto d_i^{-D} \tag{6}$$

and likewise for the next rank (the next-smaller size):

$$N(L \geqslant d_{i+1}) \propto d_{i+1}^{-D} \tag{7}$$

Because the number of fragments produces by any fracture is constant (= 2), and $d_{i+1} \propto d_i$, subtracting Eq. (6) from (7) leads to:

$$N(L = d_i) \propto d_i^{-D} \tag{8}$$

Fig. 5 shows the particle size distributions displayed in terms of the *actual* number of particles of size d (not including those larger), on double-logarithmic axes. A similar trend is observed, and in this case the slope of the fractal PSD at 45 MPa is exactly 2.5, which is highlighted in Fig. 5(b). What is also revealed by plotting this data is the nature of the emerging ranks of particles. Clearly, the particle distribution is only fractal across the linear section of the grading curve, which at 45 MPa spans between 2 mm and around 0.4 mm. Ranks of particles smaller than 0.4 mm are not fully developed, and are fewer in number rather than greater, contrary to the above definition.

An interesting observation which may also be made here is that if the data in Fig. 5(a) is plotted in terms of *percentage* of particles, as presented in Fig. 6(a), then it can be seen that percentage of any one particle size never exceeds more than approximately 20% of the total number. Moreover, the most numerous particle rank consistently comprises almost exactly 21% of the total particles, regardless of the actual particle size. It would appear that any emerging particle size increases in number until constituting approximately 21% of the total number. At this point, the rank then ceases to grow in number, and as such the overall percentage of this rank begins to decrease, as more numerous smaller particles come in to existence. The rank subsequently becomes, and remains fractal as the percentage continually decreases.

The actual quantities of each various size of particle can be compared perhaps more naturally if the data is plotted on linear axes, which is given in Fig. 6(b). The same trend as above can be seen, i.e. starting at the largest particles, (d_1 = 2 mm), the subsequent (smaller) ranks increase in quantity, reaching a peak, after which the subsequent ranks display a rapidly decreasing quantity. This trend occurs from 20 MPa onwards. At 45 MPa, the simulation was terminated due to it becoming too computationally cumbersome. At this point there were 157 particles of size d_1, with each subsequent rank increasing in quantity up to d_8 (0.4 mm), for which there are 5406 particles. The following ranks display *decreasing* quantities of particles, with just 2 of the final size d_{15} (0.079 mm). Although the total number of particles at this stage, 25,527 does not seem overtly problematic, the computational timestep is proportional to the square-root of the mass of the smallest particle, so very small particles cause the timestep to become very small [4].

Recalling Eq. (7), assuming D = 2.5, and considering particle volume ($\propto d^3$) the total volume of a given size of particle can be expressed as:

$$V(L = d_i) \propto N(L = d_i) * d_i^3$$
$$V(L = d_i) \propto d_i^{0.5} \tag{9}$$

The above relationship for the simulation is plotted in (a), in terms of the volume of each particle size against d, which shows the data at 5 MPa intervals throughout the simulation. For simplicity, the volume is represented in terms of percentage in (a), while Fig. 7 (b) shows the final set of data (obtained at 45 MPa), plotted in terms of actual volume, with a trend line indicating the slope of 0.5. The agreement shown by the data in (b) also confirms a fractal dimension of 2.5—as the gradient of the linear PSD in such a plot is equal to (3 − D) [18]; however the agreement only holds for the fully developed ranks of particle. It is worth noting the tiny volume of the smaller particle sizes: sizes 0.079–0.31 mm constitute 40% of the total particles, but approximately just 3% of the total volume/mass.
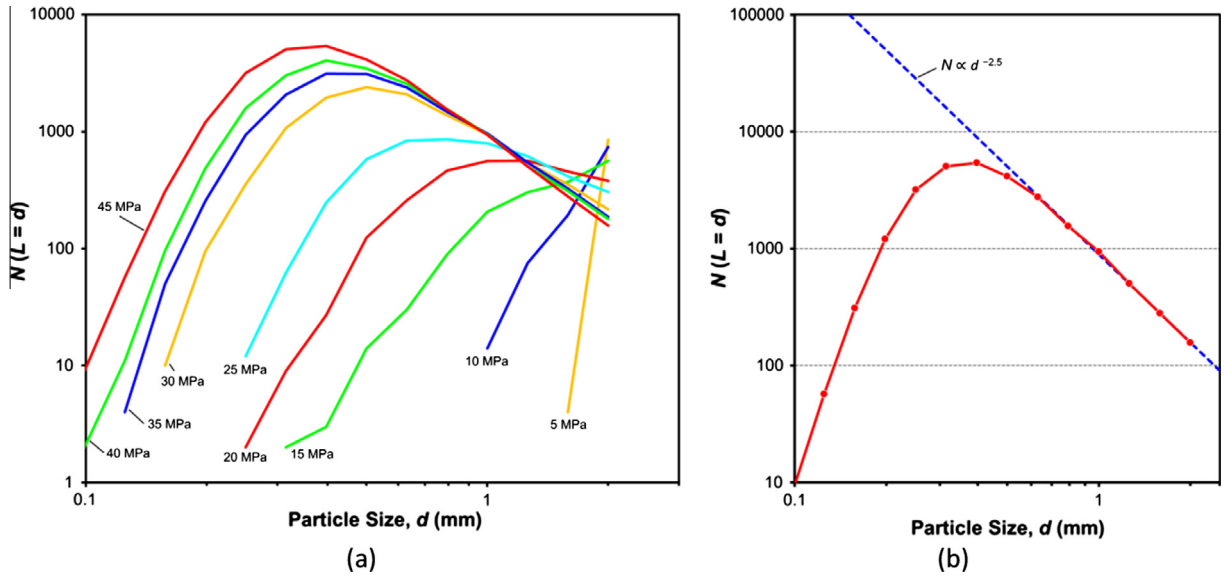
Fig. 5. Number of particles plotted as a function of particle size, throughout the simulation (a) and at 45 MPa (b).
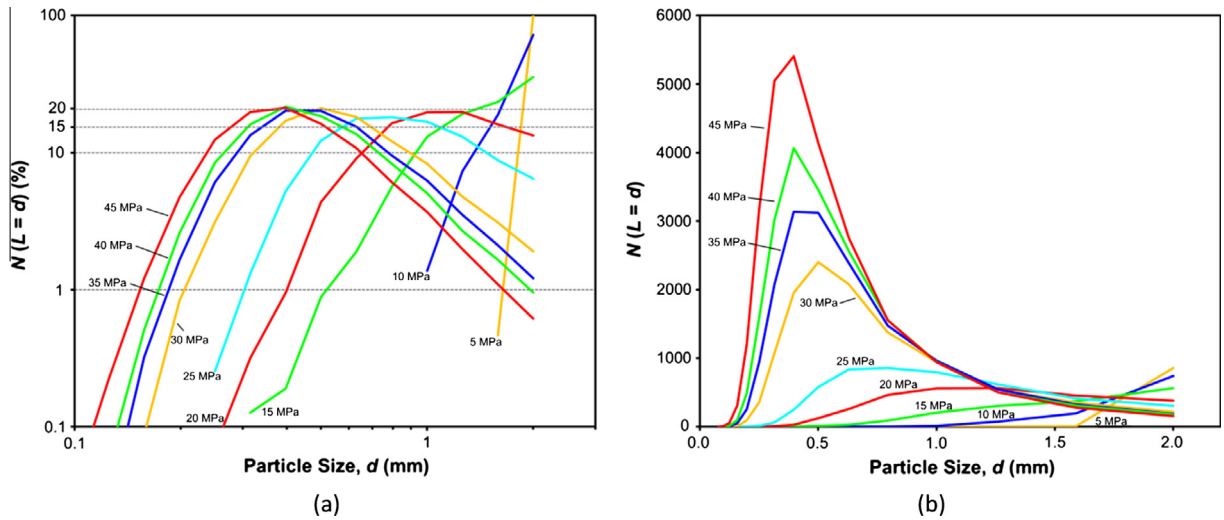

Fig. 6. Number of particles plotted as a function of particle size, in terms of percentage (a) and on linear axes (b).

5. Smallest particle size

The first hypothesis used in arriving at the compression law in Eq. (1) was that the current macroscopic stress is proportional to the strength of the smallest particles:

$$\sigma_v \propto q_{0,s} \tag{10}$$

and recalling that strength is a function of size according to Eq. (3) ($\propto d_s^{(-3/3.3)}$), the current vertical stress can be related to the size of these smallest particles:

$$\sigma_v \propto d_s^{-(3/3.3)} \tag{11}$$

These equations can be easily checked in the simulation; if the strengths of the smallest particles are proportional to the vertical stress, then the smallest particle size will follow the relation given in Eq. (10), and vice versa. However, as can be seen throughout Figs. 4–7, a clear distinction can be made in the simulations between the actual, absolute smallest particle size and the smallest *fractal* particle size. The absolute smallest particle size, denoted as

d_{sa} corresponds to the smallest particle(s) in the sample, which can be seen does not conform to the ideal linear slope of the fractal distribution. Hence it would be more appropriate to check the above relations using the smallest fractal size of particle, denoted d_{sf}—which will be taken to be the smallest particle size that lies on the linear, fractal section of the PSDs in Figs. 4–7. As an example, at 45 MPa, the absolute smallest particle size, d_{sa}, is 0.079 mm; the smallest fractal size, d_{sf}, is 0.63 mm. This is labelled in Fig. 7(b). Incidentally, the smallest fractal particle size regularly constitutes approximately 15% of the total number of particles; by drawing a horizontal line through 15% on Fig. 6(a), the point of intersection with each curve roughly indicates the smallest fractal particle size. The two quantifications of smallest particle size are plotted against vertical stress in Fig. 8(a). It is evident here that the size of the smallest fractal particles, d_{sf}, decreases in magnitude intermittently, but overall does show acceptable agreement with the above equation; a trend line (with an exponent of −1.1) is shown. The size of the absolute smallest particle(s), d_{sa}, likewise decreases during compression but does not follow the correct behaviour according to Eq. (10). This suggests that the above equations apply to the
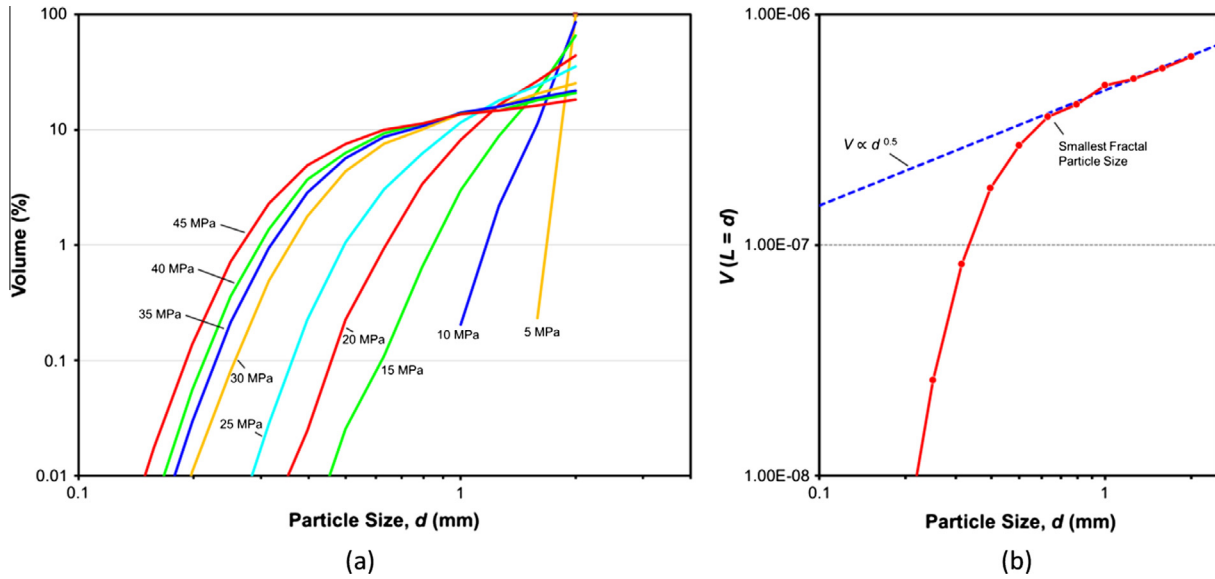
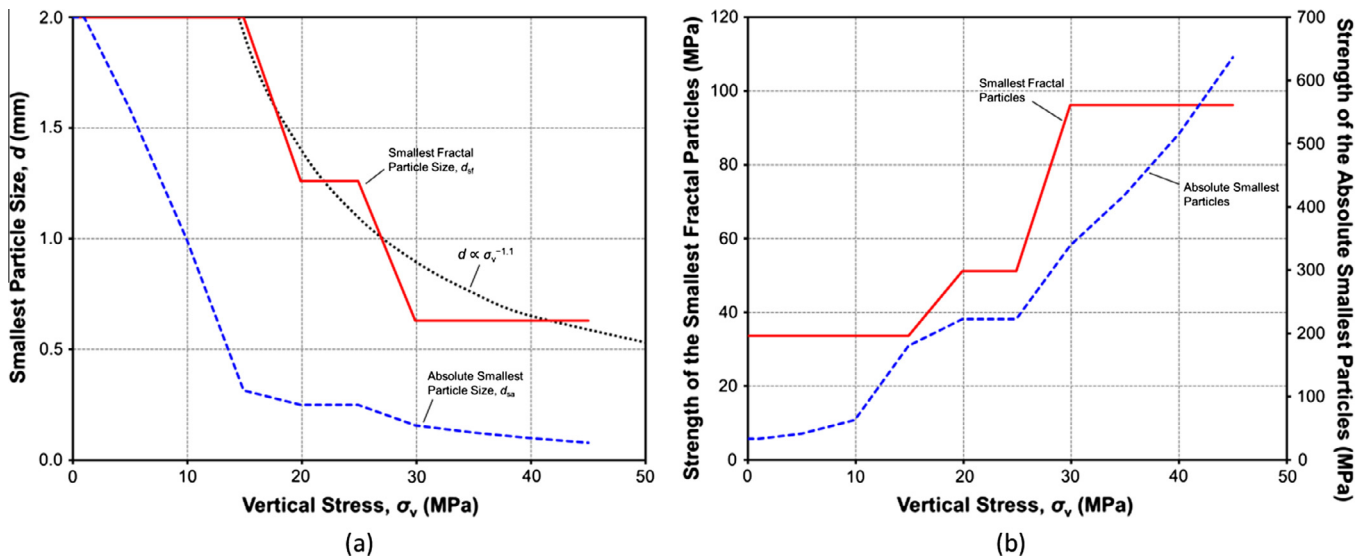**Fig. 7.** Total particle volume as a function of particle size, progressively (a) and at 45 MPa (b).

Fig. 8. Smallest particle size as a function of vertical stress (a) and strengths of the smallest particles as a function of applied stress (b).

smallest fractal particle rank. The corresponding characteristic strengths of these two classifications of smallest particles are given in Fig. 8(b). The strengths of the smallest fractal particles here should show proportionality (through the origin) with vertical stress, and although the strength of the smallest fractal particles shows the correct overall trend, the data is very discontinuous in nature.

The above results therefore suggest that it is the smallest fractal particle size, d_{sf}, which is most suitable to be considered as the smallest particle size. This is because d_{sf} conforms to the fractal PSD, so therefore correlates with N and V according to Eqs. (4) and (8), as well as the vertical stress σ_v, according to Eq. (10).

To further substantiate that the material is fractal, and behaving in accordance with the above relations, it is possible to trace the total number of particles. For a fractal distribution, putting d_s into Eq. (4) gives the total number of particles. Using the fractal dimension $D = 2.5$, rearranging, and substituting into Eq. (10) leads to:

$$N(L \geqslant d_s) \propto \sigma_v^{2.75} \qquad (12)$$

This relation is plotted in Fig. 9, which displays the total number of particles in the sample as a function of applied stress. A trend line with a slope of 2.75 is shown in this logarithmic plot, and can be seen to fit the data very well. Not only does this graph confirm that the fractal sample exhibits the correct behaviour, it indicates that it does so from a vertical stress of approximately 10 MPa onwards, i.e. the yield stress.

6. Voids ratio

The behaviour discussed above suggests that the size of the smallest fractal particles, d_{sf} can therefore be inferred from the current vertical stress according to Eq. (10), as shown in Fig. 8(a). Eq. (8) states that in a fractal distribution with a dimension of 2.5, the total volume of particles of a given size is proportional to the square-root of the diameter. Putting d_{sf} into Eq. (10), then rearranging and substituting into Eq. (8) provides a link between
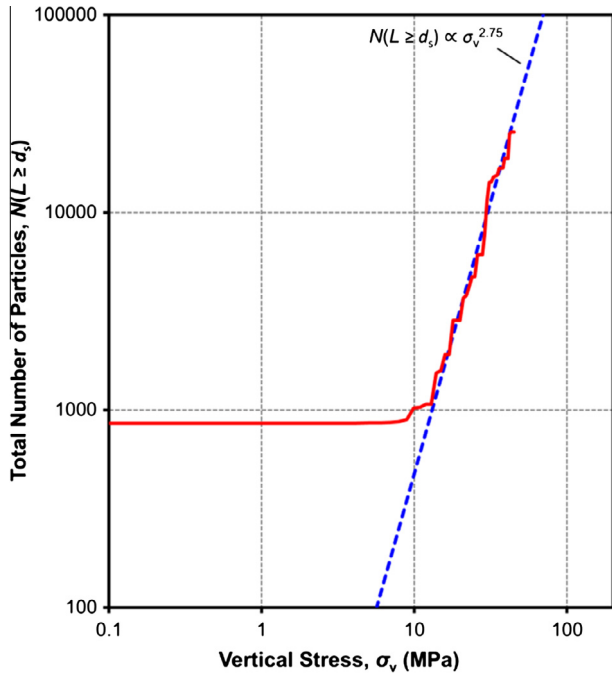
Fig. 9. Total number of particles as a function of vertical stress.

Fig. 10. Volume of the smallest fractal particles in relation to voids ratio.

the current stress and the volume of the smallest fractal particles, which can be approximately written as:

$$V(L = d_{sf}) \propto \sigma_v^{-0.5} \tag{13}$$

The *fundamental* assumption in the compression law is that the volume of the smallest particles is directly proportional to the volume of voids, and therefore, the voids ratio, e:

$$V(L = d_{sf}) \propto e \tag{14}$$

thus:

$$e \propto \sigma_v^{-0.5} \tag{15}$$

which is the slope of the NCL on logarithmic axes (Fig. 1). However, if the voids ratio is proportional to the volume of the smallest fractal particles then, recalling Eq. (8):

$$e \propto d_{sf}^{0.5} \tag{16}$$

where d_{sf} is the diameter of the smallest fractal particles. The evident problem with this is that smallest fractal particle size does not decrease in a continuous manner, as was shown in Fig. 8(a), therefore this equation fails to account for the continuous decrease in voids ratio witnessed during normal compression. In addition, physically checking the assumption in Eq. (13), by comparing the volume of the smallest fractal particles with the voids ratio does not show a comprehensive correlation. The volume of these particles, as a function of voids ratio is plotted in Fig. 10. Although the total volume of the smallest fractal particles does decrease during the simulation, as does the voids ratio, there does *not* appear to be a direct proportionality between them. Moreover, the volume of these particles at times *increases*, which is clearly in contradiction of a continuous decrease in voids ratio. To exemplify this, between 30 and 45 MPa (when $e \leqslant 0.5$), from Fig. 8(a) it can be seen the size of the smallest fractal particles is constant at 0.63 mm, during this increment the quantity, and therefore total volume of these particles increases (Figs. 5–7), whilst the voids ratio decreases. Furthermore, even though the smallest fractal size of 0.63 mm does not change during this time, the percentage of mass finer than 0.63 mm increases by almost 9% of the total mass (Fig. 2). By only
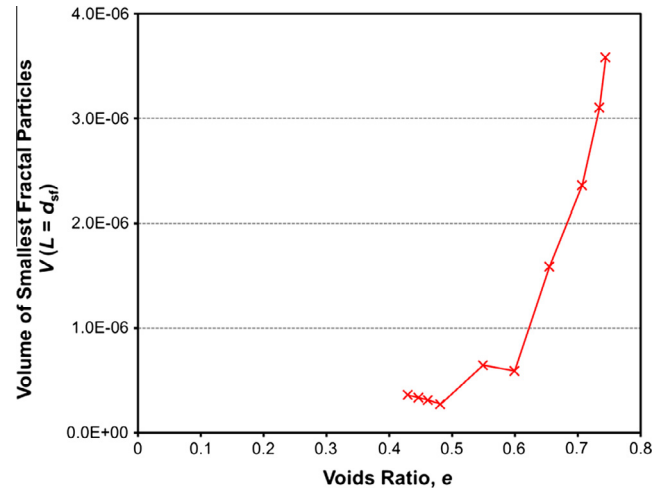
focusing on the smallest fractal particles, this change goes unaccounted for, but will inevitably have an influence on the voids ratio. It therefore seems that a more intricate definition of the 'smallest' particles is required in an evolving particle size distribution, which has constantly emerging sizes. This will be addressed in the following sections. Despite this, it can be said Eqs. (9)–(11) hold true, and the macroscopic behaviour agrees with that predicted by the compression law.

7. Particle stresses

An advantage of using DEM is the ability to observe and measure discrete variables such as contact forces and particle stresses. Particle stresses (PFC3D will calculate the stress tensor for a loaded sphere) result from the contact forces exerted on the particles, and given in Fig. 11 are cross-sectional views of the sample at various stages throughout the simulation, which display the contact forces on a central vertical plane at 5 MPa intervals. The thickness of each black line indicates the magnitude of the contact force. In Fig. 11 (a), at 5 MPa, the maximum contact force shown is approximately 64 N. In (b), taken at 10 MPa, the contact forces are noticeably greater in magnitude—the largest force in this image is 181 N. Beyond this stress, i.e. across (c)–(i), the quantity of contacts increases greatly as the number of particles increases due to crushing, the result in Fig. 11(i) being a dense network of force chains. However, during this time, the magnitude of the largest contact force does not increase significantly, despite the vertical applied stress increasing from 10 to 45 MPa. As indicated by the thickness of the lines, the largest contact forces remain approximately constant around 200 N. What can also be observed is that once a well-graded PSD has emerged, the most prominent contact forces (i.e. the thickest black lines) do not change dramatically with crushing. For example, between images (h) and (i), there are almost 7000 breakages during this interval, however the largest contact forces remain relatively unaltered, with the key difference being a greater quantity of contacts in (i). This will be due to the fact that it is mainly the smallest particles that are breaking, which carry relatively minor contact forces—the shear stress in such particles will be high due to the few contacts and size effect on this stress (proportional to d^{-2}).

Further insight can be gained by analysing the actual particle stresses. The octahedral shear stress in each particle is monitored continuously in the event that the particle's strength is exceeded, hence it is a straightforward matter to calculate the average (mean) stress for any size of particle. Fig. 12 shows the average
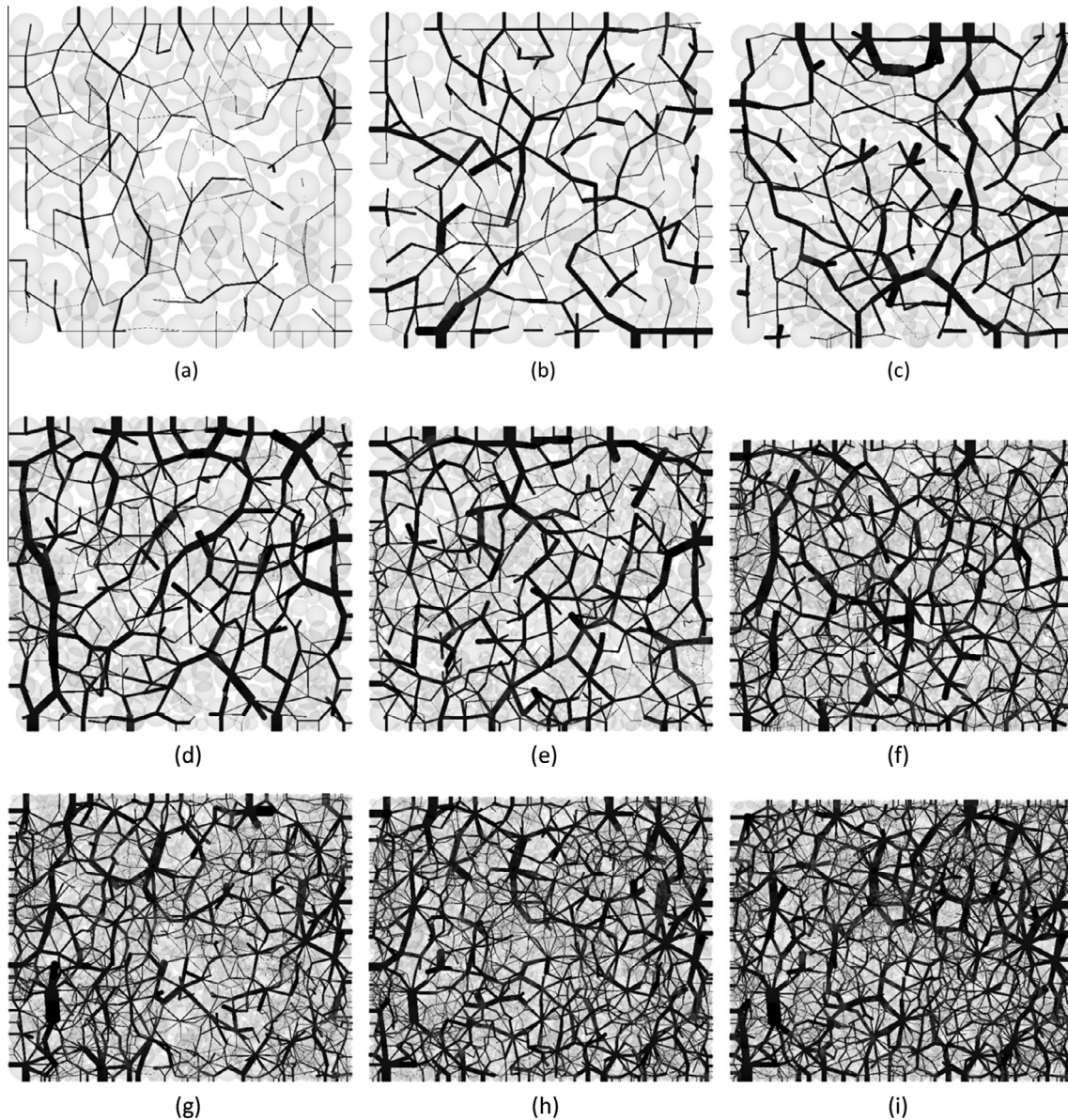
Fig. 11. Cross-sectional views showing contact forces on a central vertical plane, from 5 MPa (a) through to 45 MPa (i), at 5 MPa intervals.

octahedral shear stress, q_{av} for each of the first 6 ranks of particles (2–0.63 mm), as a function of the vertical applied stress, σ_v. Inspecting the graph shows that as soon as compression starts the average stress in the original, 2 mm-sized particles increases steadily, until some of the particle strengths are exceeded and a small number of them break. At this point—around 5 MPa—a very small number of smaller particles (d_2) come into existence. By approximately 10 MPa, an increasing number of the original d_1 particles have now broken, and the population of the next rank of d_2 particles has increased to a more significant level. The average shear stress in the original (and largest) d_1 particles increases much less rapidly from this point onwards, due to the existence of a sizable quantity of smaller particles, which provide additional contacts to the larger particles, lessening the induced shear stress. At approximately this same stage (10 MPa), a small number of the 2nd Rank (d_2) particles break, producing smaller fragments of size d_3, this process continues, and repeats itself as σ_v increases, producing smaller and smaller particles. The average stress, q_{av} for

the largest d_1 particles appears to reach an almost stable value at around σ_v = 25 MPa, beyond which there is little further increase with increasing σ_v. The average stress for any rank follows a similar trend: a fairly rapid increase, then increasing at decreasing rate, and appearing to approach a stable value. Consecutively smaller sizes ultimately bear increasingly larger stresses (compare the rightmost points of the 6 curves). The stage at which the rate of increase of average stress for any given rank begins to reduce seems to be associated with the rank becoming fully developed, at which point there will be a much greater quantity of *smaller* particles. It also corresponds with what was observed earlier in Fig. 5, that the quantities of fractal particles become stable. Although the average shear stresses are only shown for the first 6 ranks of particles (for clarity), similar behaviour is evident across the entire range of particle sizes. These observations are consistent with those made from Fig. 11—for the shear stress in the largest particles to increase, which are surrounded by many contacts, they would need to be exposed to a few very large, anisotropic contact
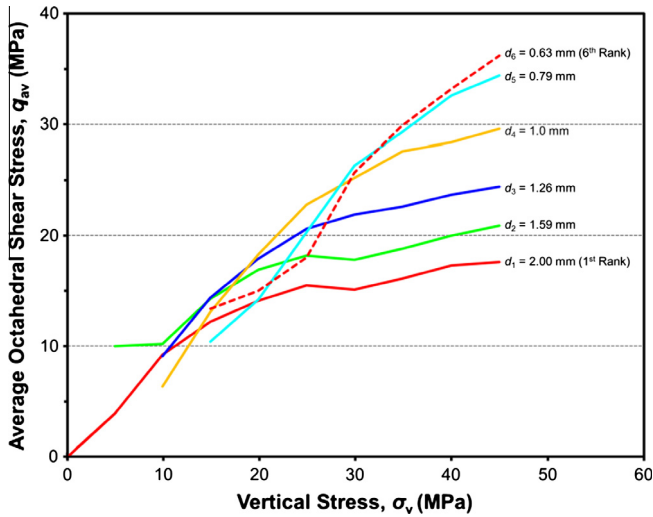
Fig. 12. Average shear stress for the first 6 particle ranks as a function of vertical stress.

forces. As was shown in Fig. 11, the magnitude of the largest contact forces ceases to increase significantly with increasing vertical stress.

Fig. 13(a) represents similar data but in this case shows the average particle stress, q_{av} as a function of particle size. It provides a snapshot of the distribution of average particle stresses at various stages of compression; each data curve represents a given macroscopic vertical stress. The overall trend for any particular data curve shows that the average particle shear stress increases with reducing particle size—however for the smallest few particle sizes (i.e. those that have not fully developed) the average stress then decreases quite rapidly with reducing particle size. However, this is somewhat misleading; the reason the smallest few ranks of particle display lower average stresses is not due to these particles simply having smaller induced stresses, but rather due to a significant proportion of them not being in a state of stress—i.e. not having any contacts, and carrying no load, whilst those that *are* stressed are in fact under a significant shear stress. This only applies to the ranks of particles that are not fully developed. The reason that many of these particles have no contacts is due to

the simulations not applying gravitational acceleration; if gravity was included then these 'floating' particles would come to rest with 3 contacts, resting under their own weight but still not carrying any external load. This can be shown perhaps more clearly by neglecting unstressed particles—and calculating the mean stress only considering the loaded particles, referred to here as the *mechanical* average particle stress. For example, if there are 1000 particles of size d_i, but only 900 are stressed, the *mechanical* average stress would simply be the mean stress of these 900 particles. Fig. 13(b) shows this data, in the same manner as the graph in part (a), however note the change in scale. In Fig. 13(b) one can see that the smallest particles—those that are stressed—are in fact under very large stresses. The mechanical average stress increases throughout with reducing particle size. These graphs reveal that although the *overall* average stress in the smallest few particle ranks is low—evidently it is still possible that some of these particles will be under stresses sufficiently large enough to cause breakage. Indeed, this could explain the shape of the particle size distributions in Figs. 5–7, in which there are *numerous* subfractal particle sizes. The emergence of new sizes of particles appears clearly to be a continuous and ongoing process—and the development of a particle size becoming fractal is gradual, not an instantaneous event. This highlights the limitations of simply considering an entire rank, e.g. the smallest fractal size of particle, as the smallest size.

In either of the graphs in Fig. 13, by comparing the data curves at consecutive stress increments, it can be seen that the average octahedral stress, regardless of particle size, increases with the applied stress. However, the increase in the average stress is much smaller in magnitude for the larger particles. For example, for the vertical stress increment 40–45 MPa: in Fig. 13(a) the average shear stress in particles of size d_1 (2 mm) increases by 0.3 MPa, whilst the average stress for the d_7 particles of size 0.5 mm increases by approximately 6 MPa. This large increase in stress can be mainly attributed to a reduction in the number of stress-free particles. This reaffirms what was observed in the previous figure, that the shear stress borne by the largest particles (which have more contacts) increases much less rapidly with increasing vertical stress.

Eq. (9) states that the applied stress is proportional to the strengths of the smallest (and therefore strongest) particles. Considering that when any particle breaks, the resulting fragments belong to the next-smaller size, when the smallest particle size
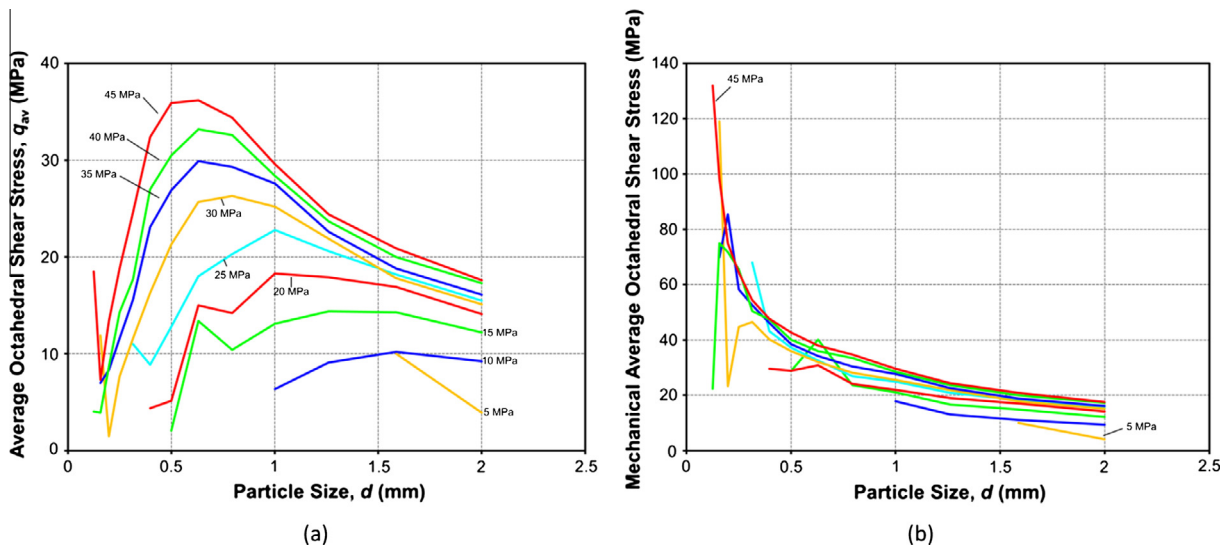

(a)   (b)

Fig. 13. Average particle shear stress as a function of particle size, overall average stress (a) and mechanical average stress (b).

decreases, it must be the smallest, and therefore statistically the *strongest* particles that are being crushed, so the applied stress must also be proportional to some statistical average of maximum particle stress. Taking the maximum particle stress as the maximum average stress exhibited by any rank, i.e. the peak values of the curves in Fig. 13(a), shows a linear relationship with the applied vertical stress, this is shown by the solid curve in Fig. 14. The maximum particle stresses shown here invariably correspond to the smallest *fractal* particle size—for example at 45 MPa, the maximum particle stress is 36 MPa, which is carried by the particles of size $d_6 = 0.63$ mm. However, by plotting this data instead of the maximum particle strengths allows a more linear correlation to be observed, as the maximum particle stress increases continuously, and through the origin—whereas the maximum particle strength is always non-zero and rises in a discontinuous manner. The fact that the largest stress corresponds to the smallest fractal particle size is hardly surprising—of the range of fractal sizes, these particles are the smallest, and will therefore have fewest contacts, and are therefore statistically more likely to be under a larger shear stress. Many of the particles smaller than this, i.e. the sub-fractal sizes, as mentioned will be stress free, thus the average stress will be lower.

A similar trend can be observed by considering the maximum *mechanical* particle stress—i.e. the peak values from Fig. 13(b). In this case, the maximum particle stresses roughly correspond with the absolute smallest particle size, and a less reliable correlation is seen with the applied stress. This data is shown by dashed line in Fig. 14.

To analyse how the distribution of stresses compare to the particle strengths (at a stress of 45 MPa), 4 sets of data are given in Fig. 15. This graph shows both measures of average particle stress, and two measures of strength—the theoretical and *actual* average particle strengths. All of these are plotted in terms of octahedral shear stress, and on logarithmic axes. The theoretical strengths are denoted by the dashed line, and follow the law given in Eq. (3). The adjacent data, denoted by the crosses, represents the *actual* mean particle strengths in the simulation for each size. The difference in these two curves reveals that due to crushing, the average strengths of the fully-developed ranks increase during the simulation. The largest difference between the theoretical and actual

mean strengths naturally occurs for the 2 mm particles. Due to the Weibull distribution of strengths, a form of 'natural selection' takes place, where the weakest particles are more likely to crush whilst the stronger, above-average strength particles are more likely to survive. Initially, before any particular rank of particle has been subjected to substantial crushing, the theoretical and actual mean strengths coincide. Hence, at 45 MPa, towards the finer end of the scale (<0.25 mm) these two curves converge, as these ranks are not fully developed and are yet to undergo significant crushing. Fig. 15 also enables the difference between the overall and mechanical average particle stresses to be visualised more clearly. By comparing the lower two curves, one can see that *for particles that are subjected to a shear stress* (dotted line), this stress increases consistently and approximately linearly (on log–log axes) with reducing size. By contrast, the *overall* average particle stress appears linear only across the range of fully developed fractal particle ranks, and the disparity for the emergent sizes (<0.63 mm) shows that a significant quantity of these small particles are not in-contact with any neighbouring particles. Nonetheless, these two curves are coincident for the fully developed ranks (2–0.63 mm), and it can be observed that the average particle stress and the average actual particle strengths appear parallel. Although not shown in Fig. 15, both of these curves exhibit a slope of approximately −0.8, so both the average particle stress and the strengths follow the same relationship with size—the average stresses for any size of particle is proportional to the average strength.

From Fig. 15, at 45 MPa the 0.63 mm particles have the largest average stress. For all intents and purposes, they are also the smallest particle size for which all particles are carrying load (the average particle stress is equal to the *mechanical* average stress). Therefore these are the *smallest* particles that, as a whole rank, are all actively in-contact with surrounding particles. These particles are also the smallest fractal particle size. This could be interpreted as implying that the voids are in some way associated with this particle size, or possibly that this size of particle represents the largest voids in the sample (if it were otherwise, a number of these particles might have no contacts and be stress free). It might therefore seem that the total void space may be a function of the volume of these particles. However, it was
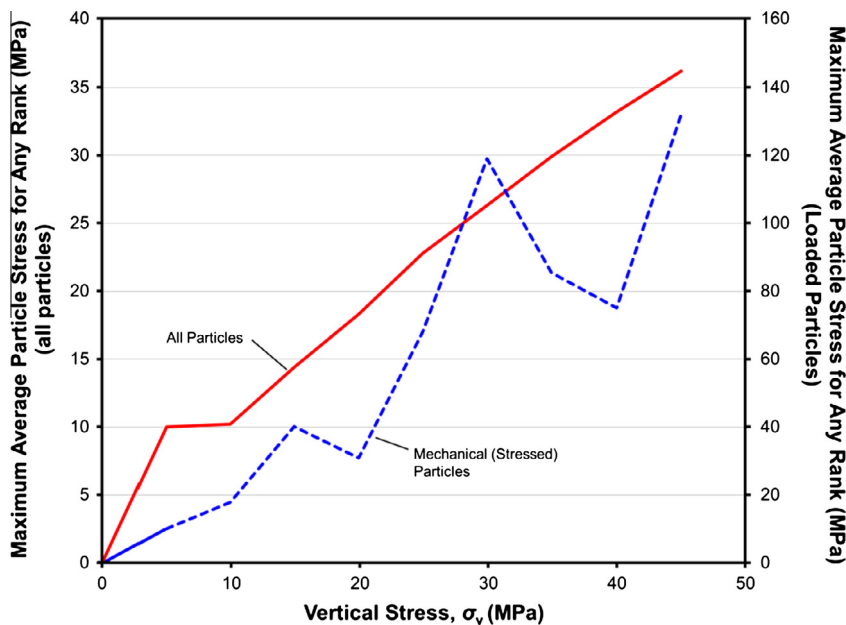

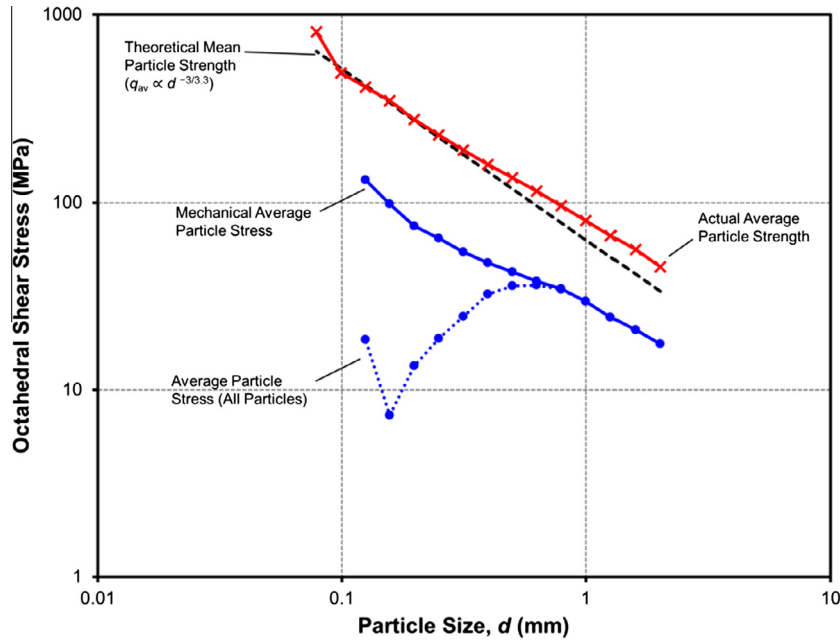**Fig. 14.** Maximum average stress of any particle rank.

Fig. 15. Comparison of stresses and strengths plotted against particle size, after compression to 45 MPa.

investigated earlier if the volume of voids was proportional to the volume of these particles (the smallest fractal particles) and this was not the case.

As mentioned earlier, a more appropriate definition of the 'smallest' particles is required. The above figures clearly show that the smallest particles are constantly changing, and that even the sub-fractal particles are crushing and producing smaller particles. At this point it seems worthwhile to consider the definition of the smallest particles to include all particles *up to and including* the smallest fractal size (e.g., at 45 MPa, all particles with $d \leqslant 0.63$ mm). The total volume of these particles however again shows no clear and robust correlation with the volume of voids, as presented in Fig. 16. The problem appears to be the abrupt change in what is considered the smallest fractal particle size. This results in a dramatic and sudden decrease in the calculated volume, which is not accompanied by an equally dramatic decrease in voids ratio.
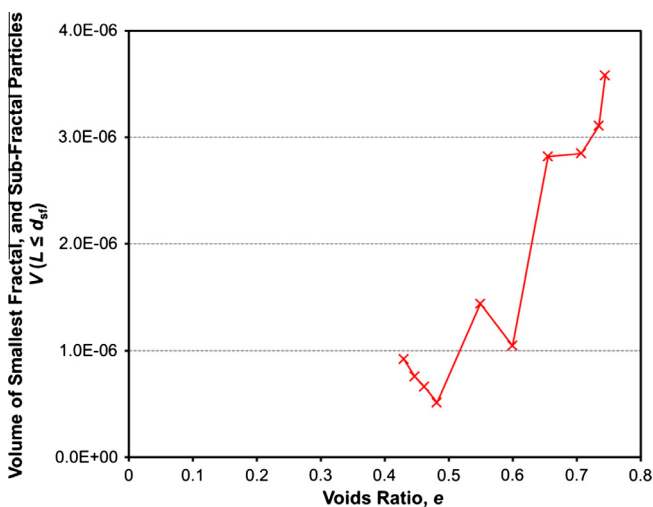
It is contended here that instead of considering the 'smallest particles' to be defined by size, there exists a group of 'critical particles' that are defined by some other means, and which determine the voids ratio. The reasoning behind this, is that whilst the smallest fractal particles may indeed represent, or be associated with the largest voids in the system, it is unlikely that all of the voids in the system of particles are equal in size, or that they become effectively smaller either *uniformly or instantaneously*. The filling of voids by newly-created fragments is a gradual, yet sporadic process. The definition of what defines and characterises these critical particles will now be discussed.

8. Coordination number

To gain further insight on what happens at the fine end of the PSD, as well as to shed more light on what characteristic might define the above-mentioned critical particles, it is possible to analyse the average coordination number of the particles. The coordination number is the number of contacts that a particle has with any neighbouring particles or boundaries; thus the *average* coordination number referred to here is the *average* number of contacts that a particle has, and again this can be analysed with respect to different ranks. The average coordination number is shown as a function of particle size in Fig. 17 on logarithmic scales, at progressive stages throughout the simulation. Firstly, it is clear to see that the average coordination number, regardless of particle size, increases with increasing vertical stress (and therefore with increasing total number of particles). What is also noticeable in Fig. 17 is that the relationship between the average coordination number and particle size shows a very consistent slope, which appears approximately linear over the fractal sizes. The slope appears independent of vertical stress, and is approximately 1.7.

Fig. 18 shows the frequency distribution of particle coordination numbers for the entire sample at the final stress of 45 MPa. The graph in (a) displays only the lower range of coordination numbers, which have the largest occurrence. As can be seen, the highest frequency corresponds to 0 contacts, which is unsurprising as the smallest particles vastly outnumber the larger particles, and as shown in Fig. 13, many of the smallest particles are unstressed.
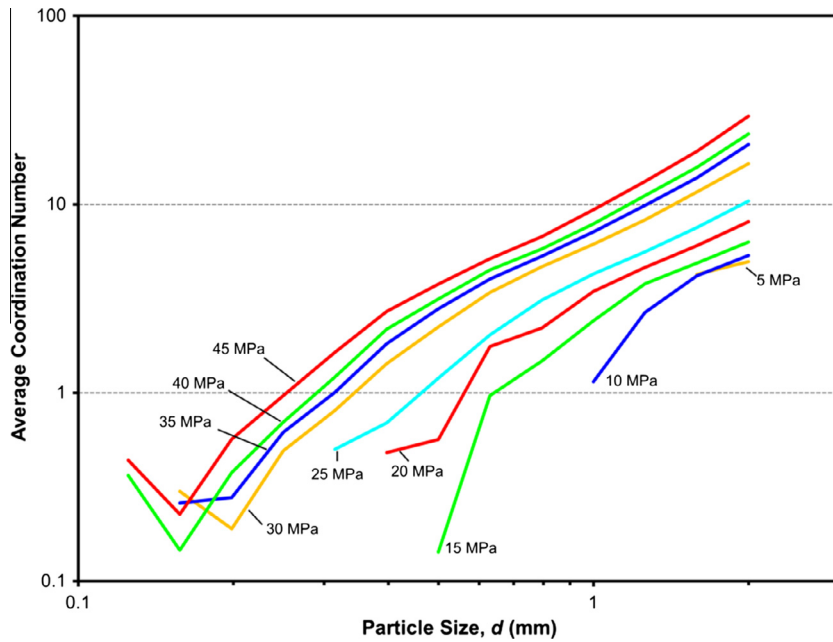

Fig. 16. Volume of fractal and sub-fractal particles in relation to the voids ratio.

Fig. 17. Coordination number as a function of particle size throughout the simulation.
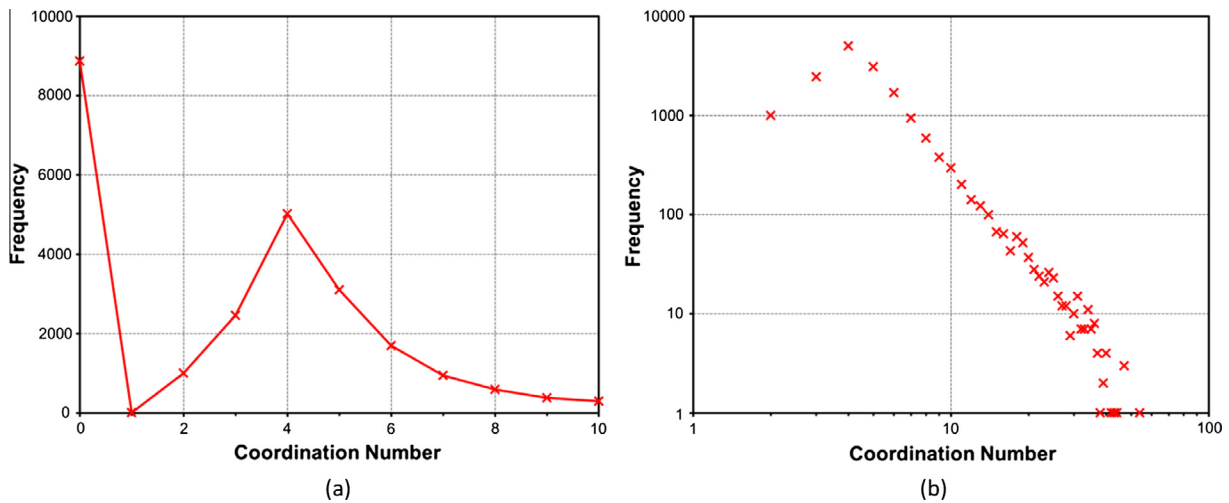

Fig. 18. Frequency distribution of coordination numbers at 45 MPa.

There are virtually no particles with just 1 contact, which makes sense as this is a transitory state—the unopposed contact force would repel the particle. Considering the particles are perfect spheres, the minimum number of contacts that one would expect a *load-carrying* particle to have is 4, and as can be seen from the graph this is second most frequent coordination number (after 0). There are also a relatively small proportion of particles with 2–3 contacts each, all of which are quasi-stationary (with low velocities). Beyond the coordination number of 4, the frequency decreases with increasing coordination number. This same data but over the full range of values is presented in Fig. 18(b), on logarithmic axes. The largest coordination number of any particle is 54, which expectedly corresponds to a 2 mm particle. There is a clear linear trend in this graph, suggesting that the frequency distribution of contacts in a fractal distribution can be expressed as a power function. The slope of this trend is approximately −3. This is a similar observation as made by Yang and Cheng [19], but in this case in three dimensions. Throughout the simulation, as crushing

progresses, the peak frequency remains consistently associated with 4 contacts, whilst the maximum coordination number in the sample increases.

9. Critical particles

It is clear from Fig. 17 that the average coordination number reduces with decreasing particle size. As mentioned above, 4 can be considered the minimum number of contacts required for a load-carrying particle to be in a stable position within the system. Therefore one would expect the smallest particles to have 4 (or fewer) contacts. These particles will not be in contact with any smaller particles (otherwise they would have more contacts), but rather equally-sized and larger particles which prevent the formation of further contacts. It is proposed here that the void space surrounding such a particle, with 4 or fewer contacts is proportional to the particle volume, and therefore that particles with a

coordination number *less than or equal* to 4 should be considered as the critical particles.

The term critical particles is used here instead of smallest particles because, whilst these particles *are* considered the smallest, they need only be the smallest particle on a *local scale*. For example, consider the sample at 45 MPa: there may exist 1 particle of size $d_6 = 0.63$ mm, which has 4 contacts, whilst simultaneously elsewhere in the sample there exists another particle of size d_6 but with 8 contacts, surrounded by smaller fragments of the emergent sizes d_7, d_8, or d_{15} (for instance). The former particle, with 4 contacts is—*locally*—the smallest particle, whilst the latter, with 8 contacts is not. Clearly, the voids around these two identically-sized particles will be different. Thus, considering critical particles, defined by their number of contacts, provides a more suitable definition than simply size alone, and enables a much more contemporaneous categorisation of particles.

When a small particle, with 4 contacts breaks, the chances are that the 2 new fragments will be small enough to fit into the void and with 4 or fewer contacts. In other words, the immediate fragments of a critical particle will also be critical, so would not *directly* contribute to a reduction in the critical volume. However, the creation of these 2 new particles provides additional contacts to the surrounding neighbouring particles, which means previously-critical particles gain contacts and become non-critical, thereby

causing a reduction in the volume of critical particles. Thus, individual particles within a rank may become non-critical at any moment, avoiding the problem of having to consider a whole rank as either critical or non-critical.

The volume of all particles with 4 or less contacts can be tracked throughout the simulation, and this measured value is now plotted against the voids ratio in Fig. 19. The correlation is clear, and strongly implies that the volume of these particles is what determines the volume of voids. The data in Fig. 19 is from a vertical stress of 10 MPa onwards, i.e. from the point when the internal stresses are large enough to initiate breakage. What is remarkable about this, is that the sample cannot be considered to have reached a fractal distribution at this point, suggesting that there is a robust relationship between these critical particles and the voids ratio. Considering that the volume of solids is constant, the voids ratio can be easily converted to give the volume of voids. Following this, the gradient of the linear relationship between the volume of critical particles and the volume of voids is approximately 0.37. This shows that for the sample used in this work, the volume of voids is approximately 2.7 times bigger than the total volume of the critical particles. Thus, this may be interpreted as on average, each critical particle (one with $\leqslant 4$ contacts) has an associated void space approximately 3.7 times larger in volume (including the volume of the particle).

The relationship observed between the volume of these critical particles and the voids ratio confirms the fundamental assumption underlying the compression law (while also showing the difficulty in defining the 'smallest particles' in a constantly evolving particle size distribution). To re-affirm this, it is possible to calculate the average, or 'effective diameter' of these critical particles. This is obtained simply by dividing their total volume by the number of particles, then finding the diameter of an equivalent sphere of this (mean) volume. This effective diameter is plotted against vertical stress in Fig. 20(a), and is shown to demonstrate excellent agreement with the relationship in Eq. (10). Likewise, Fig. 20(b) shows both the average strength and average stress of these particles, which agree with Eq. (9) and show direct proportionality to the vertical stress. Both of these graphs show more continuous and reliable correlations than in Fig. 8, which involved fixed values that were associated with a single particle size.

At any stage during compression (after yielding), there always exists sub-fractal particles (Fig. 6). As discussed earlier, many, if not all, of these sub-fractal particles will be considered critical, hence the effective diameter of the critical particles, d_e will be
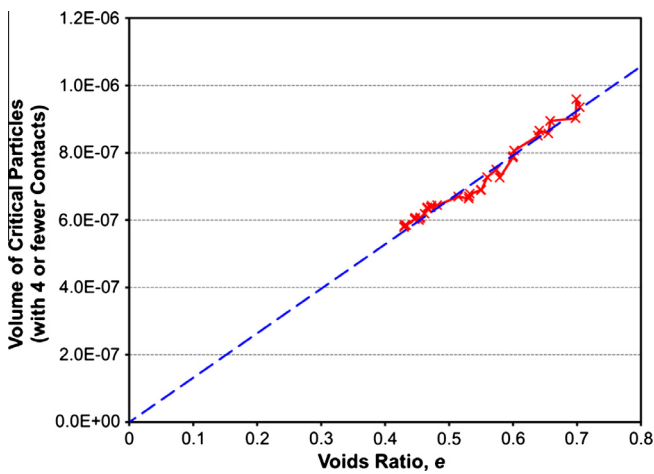

Fig. 19. Volume of critical particles (with 4 or less contacts) plotted against voids ratio.
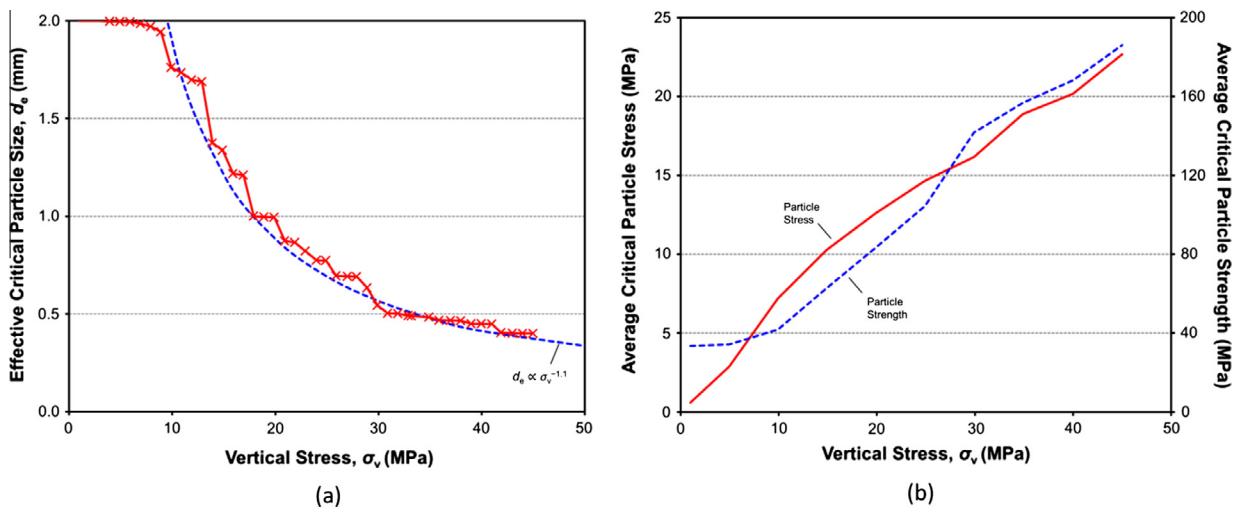

(a)

(b)

Fig. 20. Effective particle size (a) and effective particles' strength and average stress (b) as functions of applied stress.

smaller than the smallest fractal particle size, d_{sf}. Equally, this effective particle size will be larger than the *absolute* smallest particle size d_{sa} (which, as a rank is not fully-developed, and often only corresponds to a handful of particles). Clearly then the effective size of the critical particles is bounded by the absolute smallest size, and the smallest fractal particle size: $d_{sa} < d_e < d_{sf}$. The critical particles as a group consist of particles across this range.

Before yield, which occurs at approximately 10 MPa, there is a negligible amount of particle crushing, and the sample is effectively still mono-disperse and consists of only 2 mm particles. Hence $d_{sa} = d_{sf}$, therefore $d_e = 2$ mm. This can be seen in Fig. 20. Immediately upon yielding, substantial crushing initiates, which produces smaller, but as yet *non-fractal* particle sizes, so d_{sa} decreases, and therefore so does the effective particle size d_e, also clearly visible in Fig. 20. The rate of decrease in d_e with stress, as highlighted in the figure is dictated by the hardening law defined in Eq. (3).

10. Conclusions

After compression to high stresses, the numerical sample was comprehensively shown to consist of a fractal distribution of particle sizes. Progressive particle size distributions showed that at any instant during normal compression, the fractal distribution spans a finite range of sizes, and this range increases during compression. Beyond the lower end of this range of fractal particle sizes, there are numerous particle sizes in a state of development, which grow in population until becoming fractal. Any new, emerging particle size was shown to gradually increase in quantity, until comprising approximately 20% of the total number, at which point the number of particles of this size stabilises, becoming part of the fractal distribution, after which the representative percentage of these particles decreases, as new smaller sizes of particle develop (increasing the overall number of particles).

The macroscopic behaviour of the sample was consistent with prior results by the authors, and agreed with their previously published compression law. A number of assumptions inherent in the authors' previous compression law were examined in the simulation, all of which were shown to be reasonable. The average strength of the smallest fractal particle size was shown to be proportional to the vertical stress, and as such the smallest fractal particle size decreased with stress according to the size-hardening law. This meant that the total number of particles also increased with vertical stress correctly according to the evolving fractal distribution. In addition, the distribution of particle stresses, strengths and coordination numbers were analysed. For each fractal particle size, the average particle stress was proportional to the average particle strength, with both following the same relationship with particle size at the maximum applied stress. It was shown that the smallest particles, in particular those that have not yet developed and have not yet become fractal in nature (and constitute a very small overall percentage), are continually crushing, producing smaller and smaller particles.

A key assumption in the authors' previous work is the association of the overall void space with the size of the smallest particles. However, there may only be one such particle, and so this would be inappropriate. The use of the smallest fractal size was also inappropriate because many smaller particles contribute to the available void space. Therefore a suitable definition of the smallest particle to be associated with the current available void space was required. The significant outcome of this was that the void space, and therefore the voids ratio, was shown to be directly proportional to the volume of the smallest, or 'critical' particles, which were defined as those particles having 4 or fewer contacts. This relation proved to be valid from the yield stress (approximately 10 MPa) onwards (i.e. as soon as particle breakage begins) before the global particle size distribution can be said to be fractal.

This work has therefore provided a detailed study of emerging fractal distributions during normal compression and provided insight into why the established normal compression line exists, based on fractal mechanics of void compression as stress increases.

References

[1] McDowell GR, de Bono JP. On the micro mechanics of one-dimensional normal compression. Géotechnique 2013;63:895–908. http://dx.doi.org/10.1680/geot.12.P.041.
[2] McDowell GR, de Bono JP, Yue P, Yu H-S. Micro mechanics of isotropic normal compression. Géotech Lett 2013;3:166–72. http://dx.doi.org/10.1680/geolett.13.00050.
[3] de Bono JP, McDowell GR. An insight into the yielding and normal compression of sand with irregularly-shaped particles using DEM. Powder Technol 2015;271:270–7. http://dx.doi.org/10.1016/j.powtec.2014.11.013.
[4] Itasca. PFC3D; 2015.
[5] Ben-Nun O, Einav I. A refined DEM study of grain size reduction in uniaxial compression. In: 12th International conference on international association for computer methods and advances in geomechanics (IACMAG); 2008. p. 1–6.
[6] Cheng YP, Bolton MD, Nakata Y. Discrete element simulation of crushable soil. Géotechnique 2003;53:633–41. http://dx.doi.org/10.1680/geot.2003.53.7.633.
[7] McDowell GR, Amon A. The application of Weibull statistics to the fracture of soil particles. Soils Found 2000;40:133–41.
[8] McDowell GR. On the yielding and plastic compression of sand. Soils Found 2002;42:139–45.
[9] de Bono JP, McDowell GR. DEM of triaxial tests on crushable sand. Granul Matter 2014;16:551–62. http://dx.doi.org/10.1007/s10035-014-0500-x.
[10] de Bono JP. Discrete element modelling of cemented sand and particle crushing at high pressures. University of Nottingham; 2013.
[11] McDowell GR, Daniell CM. Fractal compression of soil. Géotechnique 2001;51:173–6. http://dx.doi.org/10.1680/geot.2001.51.2.173.
[12] Nakata Y, Kato Y, Hyodo M, Hyde AF, Murata H. One-dimensional compression behaviour of uniformly graded sand related to single particle crushing strength. Soils Found 2001;41:39–51.
[13] Hagerty MM, Hite DR, Ullrich CR, Hagerty DJ. One-dimensional high-pressure compression of granular media. J Geotech Eng 1993;119:1–18. http://dx.doi.org/10.1061/(ASCE)0733-9410(1993)119:1(1).
[14] Palmer AC, Sanderson TJO. Fractal crushing of ice and brittle solids. Proc R Soc A Math Phys Eng Sci 1991;433:469–77. http://dx.doi.org/10.1098/rspa.1991.0060.
[15] Turcotte DL. Fractals and fragmentation. J Geophys Res 1986;91:1921. http://dx.doi.org/10.1029/JB091iB02p01921.
[16] Steacy SJ, Sammis CG. An automaton for fractal patterns of fragmentation. Nature 1991;353:250–2. http://dx.doi.org/10.1038/353250a0.
[17] Lobo-Guerrero S, Vallejo LE, Vesga LF. Visualization of crushing evolution in granular materials under compression using DEM. Int J Geomech 2006;6:195–200. http://dx.doi.org/10.1061/(ASCE)1532-3641(2006)6:3(195).
[18] McDowell GR, Bolton MD. On the micromechanics of crushable aggregates. Géotechnique 1998;48:667–79. http://dx.doi.org/10.1680/geot.1998.48.5.667.
[19] Yang Y, Cheng YM. A fractal model of contact force distribution and the unified coordination distribution for crushable granular materials under confined compression. Powder Technol 2015;279:1–9. http://dx.doi.org/10.1016/j.powtec.2015.03.006.